Characterization of Nanosized Material Extracted from Clear Suspensions for MFI Zeolite Synthesis

Raman Ravishankar,[†] Christine E. A. Kirschhock,[†] Peter-Paul Knops-Gerrits,[†] Eddy J. P. Feijen,[†] Piet J. Grobet,[†] Peter Vanoppen,[‡] Frans C. De Schryver,[‡] Gerhard Miehe,[§] Hartmut Fuess,[§] Brian J. Schoeman,[||] Pierre A. Jacobs,[†] and Johan A. Martens*[,†]

Centrum voor Oppervlaktechemie en Katalyse and Laboratorium Moleculaire Dynamica & Spectroscopie, K.U. Leuven, Kardinaal Mercierlaan 92, B-3001, Heverlee, Belgium, Department of Materials Science, Division of Structural Research, University of Technology, Darmstadt, Germany, and Department of Chemical Technology, Luleå University of Technology, Sweden

Received: January 25, 1999; In Final Form: March 28, 1999

The silica species contained in an aged clear suspension, which upon heating gives rise to the crystallization of Silicalite-1, were extracted with 80% efficiency using a sequence of acidification, salting out, phase transfer into organic solvent, and freeze-drying methods. This silica powder was characterized by X-ray scattering, transmission electron microscopy, atomic force microscopy, and ^{29}Si magic angle spinning nuclear magnetic resonance. These techniques gave evidence for the presence of a very specific morphology, corresponding to slab shaped particles, with dimensions of 1.3 × 4.0 × 4.0 nm. The nanoslabs have the MFI structure with nine channel intersections per particle, each containing a TPA cation. The identity of the extracted nanoslabs with the species in suspension is evidenced with in situ and ex situ X-ray scattering.

Introduction

Although zeolites are widely used as catalysts and adsorbents, little is known about the crystallization mechanisms of these microporous crystalline oxides. To optimize zeolite performance and synthesis it is essential to understand the mechanisms responsible for their formation.

The zeolite Silicalite-1, a silica polymorph with MFI topology and first reported by Flanigen et al.[1] in the early 70s, can be synthesized either by the traditional hydrothermal gel method or from a so-called "clear solution".[2−4] Many studies on the gel and clear solution processes were undertaken to elucidate the mechanism of MFI synthesis. By now a stepwise mechanism seems to be emerging from these efforts: The initial formation of a precursor leads to the formation of a nanoscopic species with well-defined size. These entities already are observed before heating of the reaction mixtures studied and are present during the formation of a growing fraction of final crystals at elevated temperatures.

A clear solution synthesis starts with the hydrolysis of tetraethyl orthosilicate (TEOS) in a concentrated, aqueous tetrapropylammonium hydroxide (TPAOH) solution at room temperature. The product of this clear solution procedure usually consists of particles between 100 and 230 nm[4,5] and is referred to as "colloidal Silicalite-1". TEOS ensures the silicon to be present in monomer form, thus circumventing the primary dissolution of the polymeric silica source required in the gel method. The TPA^+ cation serves as template, directing the hydrolysis and condensation processes towards the MFI structure.[6,7] The presence of an initially formed polysilicate species in close contact with the template and already containing characteristics of the MFI structure has been proposed for a long time.[8−11] These precursors should then give rise to larger entities and the final product. This is achieved by heating the clear solutions from room temperature to 100 °C. Several authors have studied this aspect of MFI formation.[12−18] The evolution of particle sizes was monitored by the scattering of light (DLS),[12−14] X-rays (SAXS),[14−18] or neutrons (SANS).[14] All authors agree on the formation of a small species of nanoscopic dimensions (3−5 nm) with a more or less internally ordered structure resembling the final MFI product. Although globular or cylindrical geometry was attributed to these structures during the evaluation of the SAXS and SANS data, the exact nature of these particles, conveniently termed "nanoblocks", remains unknown.

The nanoblocks can be extracted from the clear solutions even before heating[19,20] and handled as a powder. According to decoupled ^{13}C MAS NMR[20] it contains TPA and its IR spectrum resembles that of bulk Silicalite-1, but no Bragg crystallinity can be detected.[19,20] In the catalytic epoxidation of 1-hexene and the hydroxylation of phenol, a specimen doped with titanium exhibits molecular shape selectivity similar to TS-1 catalyst, the titanosilicate analogue of Silicalite-1.[20]

The formation of larger intermediates in the crystallization process was observed by several authors.[14,15,17−19] The role of the nanoblocks in their formation remains unclear. Whereas a fractal growth pattern is favored by one group,[17,18] others prefer an aggregation mechanism,[14,15] or even claim the dissolution of nanoblocks into precursors as a nutrient reservoir.[21] The fact is that the nanoblocks are present throughout the crystallization process,[14,22] which in itself rather hints at a successive aggregation.

In the present paper, the characterization of the nanoblocks and a proposal for their structure are presented. The solids isolated from solution were studied with ^{29}Si magic angle

* Corresponding author telephone, 0032-16-321637; fax, 0032-16-321998; e-mail, johan.martens@agr.kuleuven.ac.be.
[†] Centrum voor Oppervlaktechemie en Katalyse.
[‡] Laboratorium Moleculaire Dynamica & Spectroscopie.
[§] University of Technology.
[||] Luleå University of Technology.

10.1021/jp990296z CCC: $18.00 © 1999 American Chemical Society
Published on Web 05/27/1999

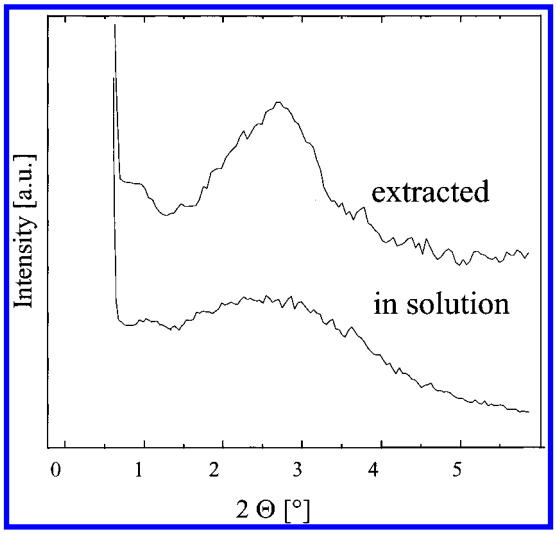

Figure 1. Low angle X-ray scattering between 0.25° and 7.75° 2θ, of the clear suspension, compared to that of extracted powder with 5× increased intensity.

spinning nuclear magnetic resonance (MAS NMR), dynamic light scattering (DLS), low angle X-ray scattering (XRS), atomic force microscopy (AFM), and transmission electron microscopy (TEM). These nanoblocks play a crucial role in the crystallization process. The follow-up articles[23,24] will deal with the nature of the precursor species, the mechanism of the formation of the nanoblocks from the precursors, and their transformation into colloidal Silicalite-1.

Experimental Procedures

The in situ low angle X-ray scattering (XRS) experiments were carried out with Cu−$K_{\alpha 1}$ radiation in a STOE Stadi P diffractometer with transmission geometry using capillaries of diameter 0.75 mm.

TEM investigations were carried out with a 200 kV Philips CM200 Ultra Twin apparatus, characterized by a point-to-point resolution of 0.19 nm. The powder was deposited on a holey carbon film. By choosing intermediate magnifications, the beam damage could be minimized.

A Discoverer AFM system (TMX 2010, TopoMetrix Inc., Santa Barbara, CA) is operated in noncontact mode using high frequency (310−380 kHz) cantilevers and amplitude detection. Cantilevers were equipped with a pyramidal Si_3N_4 tip with a radius of curvature of less than 50 nm. Powders were dispersed in chloroform, cast on mica plates, and evaporated.

^{29}Si MAS NMR was performed at 59.6 MHz, in a 7 mm double-bearing probe spinning at 4 kHz, using $\pi/6$ tip angle pulses, 3,000 transients, and 60 s recycle delay to allow complete relaxation. ^{29}Si CP-MAS NMR was performed with a contact time of 1 ms and 3 s recycle delays.

Results and Discussion

Isolation of Nanoblocks. To prepare an aqueous suspension of nanoblocks, the procedure of Shoeman and Regev[25] was adapted. An amount of 9 g of tetraethyl orthosilicate (TEOS) was added under vigorous stirring to 7.9 g of a 40% aqueous solution of tetrapropylammonium (TPA) hydroxide. After 30 min, 9 g of water was added and stirring continued for 24 h. A clear suspension was finally obtained which can serve as mother liquid for the crystallization of colloidal Silicalite-1.[26] DLS on this suspension revealed the presence of particles with a uniform size and a characteristic length of 2.8 nm, assuming monodispersity in size.[25] The in situ X-ray scattering (XRS) pattern of this suspension shows a maximum at 2.8° 2θ (Figure 1), confirming the presence of well-defined nanoscopic particles.

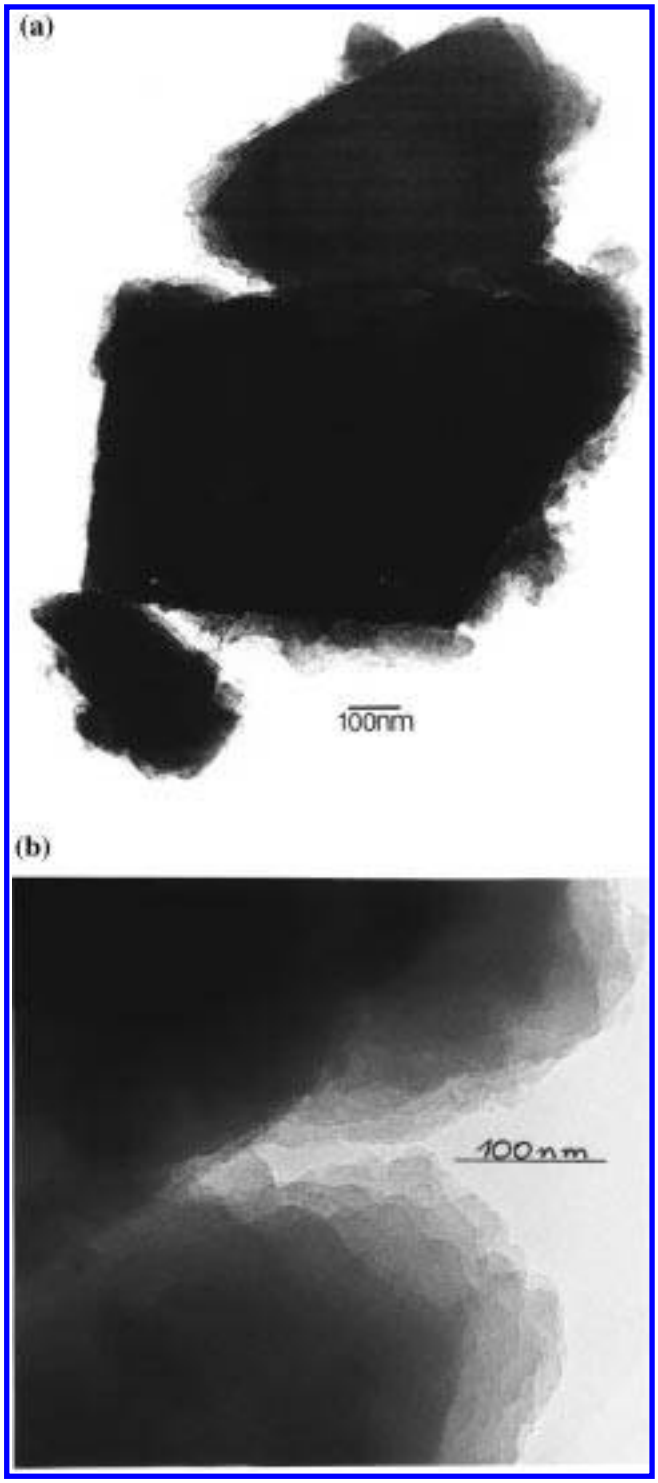

Figure 2. TEM pictures of extracted powder: (a) Evidences for the straight edges and right angles and (b) layered structure close to the edges of the larger aggregates.

Isolation of solid material from the clear suspension was done by cooling to 273 K, acidification to pH 3 using HCl, and addition of *tert*-butyl alcohol and sodium chloride as hydrogen bonding and salting-out agents, respectively. After freeze-drying of the organic phase, a white powder was obtained in a yield on silica basis of 80%. The XRS of the isolated solid was similar to that of the suspension (Figure 1), ensuring the solid to be composed of the same entities present in the clear suspension

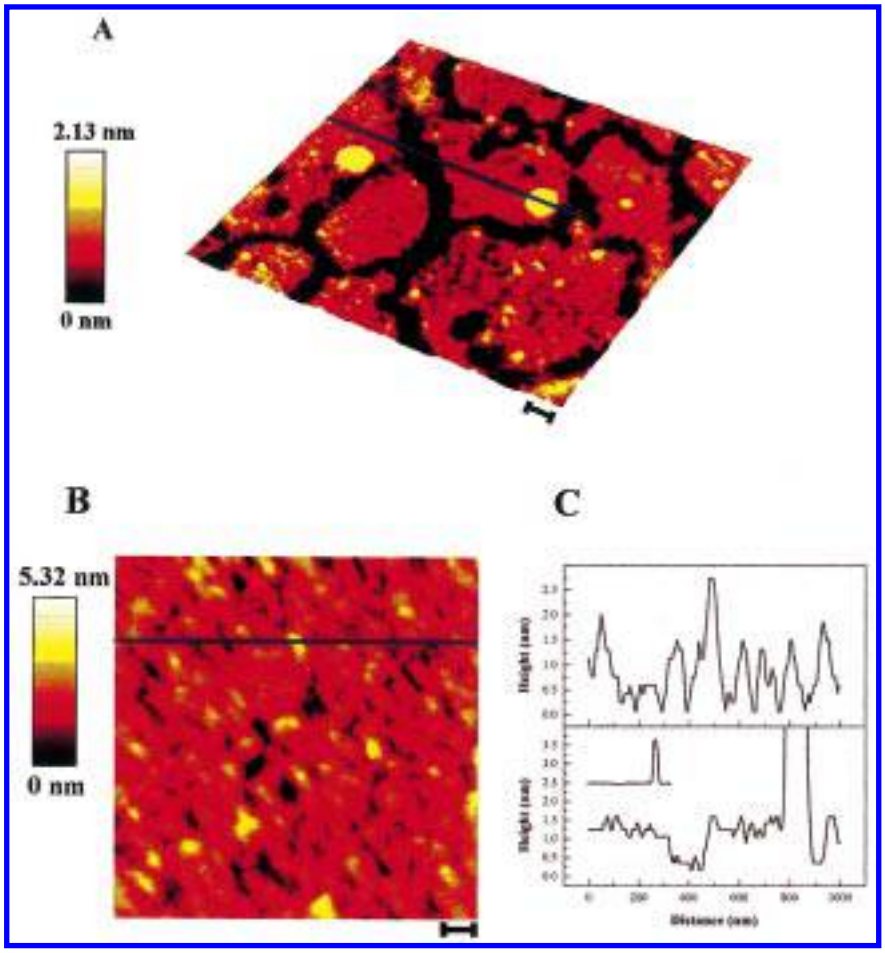

Figure 3. 3D and 2D AFM noncontact images ((A) and (B)) and selected line scans (C) of evaporated films of extracted powder. The black scale bars in (A) and (B) correspond to 100 nm.

and corresponding to the nanoblocks. The extracted solid can easily be redispersed in water to give a clear liquid, containing nanoblocks of the same size as before. A detailed analysis of the in situ recorded XRS patterns at low angles will be presented in one of the follow-up papers.[24]

TEM. Transmission electron microscopy shows the extracted powder to appear as rather large blocklike structures (Figure 2a). These display straight edges and right corners throughout the sampled material. Closer inspection of the edges reveals these blocks to have a layered structure (Figure 2b). Although these regions quickly disintegrate in the electron beam of the microscope, it is again possible to conceive the same building characteristics of straight edges and right angles in the thin layers as in the larger structures they are building. The nanoblocks could not be detected as separate entities by TEM. This either is due to their fragile constitution or to the formation of an aggregate upon extraction, corresponding to the large blocks observed. The individual layers assumed to be the nanoblocks and composing the aggregates have rectangular characteristics and, therefore, will be termed "nanoslabs".

Despite the regular, structured appearance of the extracted powder in TEM, it is lacking Bragg diffraction. This is to be expected for a physical aggregate of small entities, which themselves are well ordered but too small to allow for coherent scattering.[9] Also, the TEM studies did not provide any evidence for crystallinity, supporting the loose nature of the aggregation.

AFM. AFM pictures of the extracted powder redispersed in chloroform and deposited on a mica surface by evaporation show, besides the aggregates observed by TEM (Figure 3A), also their individual building units (Figure 3B). The aggregates appear in Figure 3A as large yellow dots, embedded in an evaporated discontinuous film of nanosize particles. Characteristic step heights of 1.2 ± 0.3 nm are common for the surface of the large blocks as well as the surrounding surface as shown in the two selected line scans (Figure 3C). Occasionally, the double or triple height of an individual step of 1.2 nm is observed, indicating the ability of the nanoslabs to stack. Therefore, with the information of the rectangular geometry of the nanoslabs gleaned from the TEM investigation, this length can be assigned to the thickness of a nanoslab.

A similarly stepped surface has been seen during the investigation of colloidal Silicalite-1 crystals[26] formed from these clear suspensions. The observation that the same step height is characteristic for the crystallization product suggests an active role of nanoslabs in the crystallization process.

NMR. ^{29}Si MAS NMR (Figure 4) reveals the presence of three lines, assigned with the help of intensity enhancements under cross polarization (CP) to Q^4 (-110 ppm), Q^3 (-101 ppm), and Q^2 (-92 ppm) with relative intensities of 51.1, 40.6, and 8.3%, respectively (Figure 4). The ^{29}Si MAS NMR line widths are comparable to those of MCM-41, a mesoporous semicrystalline silica[27] (Figure 4), but smaller than in Aerosil, representative of amorphous silica (Figure 4). The size and shape of the particles were modeled by cutting spherical, cubic, or slab-shaped volumes with variable dimensions from a giant silicon dioxide cluster with MFI structure[28] with randomly changing positions and orientations with respect to the crystallographic directions *a*, *b*, and *c*. The relative concentrations of Q^2, Q^3, and Q^4 silicons in such spheres gave a best fit to the experimental Q^n distribution derived from ^{29}Si NMR for a

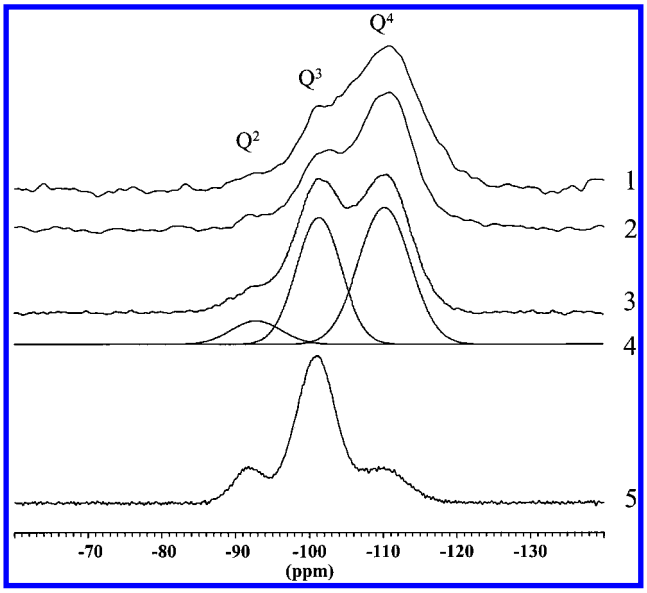

Figure 4. Comparison of ^{29}Si MAS NMR spectra of: (1) Aerosil, (2) MCM-41, (3) Silicalite-1 nanopowder as obtained, (4) after deconvolution, and (5) with ^{29}Si CP-MAS NMR of extracted powder.

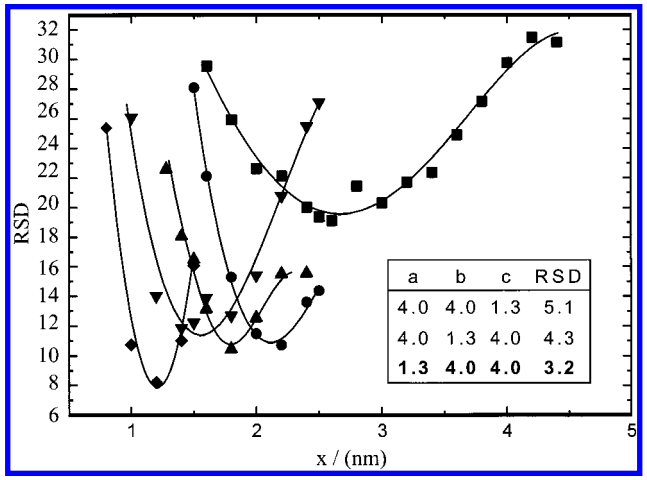

Figure 5. Root square deviation (RSD) of the fit of the Q^n distribution for model nanoparticles with MFI topology to the experimental Q^n distribution from ^{29}Si MAS NMR. Squares, spheres with diameter x; Circles, cubes with vertex x; Triangles, slabs with $x = y = z/2$; Inverted triangles, slabs with $x = y/2 = z/2$; Diamonds, slabs with $x = y/4 = z/4$. The impact of the orientation of the slabs is illustrated in the inset for optimized slab dimensions.

diameter of 2.5 nm, in good agreement with the hydrodynamic diameter determined with DLS (2.8 nm)[25] but with large root square deviation (RSD) (Figure 5). Whereas with cubes an improved fit was obtained (for 2.2 nm cubes, RSD = 11.5), RSD was substantially better with slab-shaped particles, in accordance with the TEM and AFM results. The inset in Figure 5 shows that fitting was extremely sensitive to the orientation and cut of the slab. The best fit was obtained with slabs of 4.0 nm according to the *b* and *c* crystallographic axes of the MFI topology, and of 1.3 nm according to the *a* direction. The structure of the best fitting nanoslabs is shown in Figure 6. They have three straight channels parallel to the *ac* plane, intersected by nine short channel segments, representing the zigzag channels of the MFI topology. To account for the possibility of internal defect sites, the same calculations were repeated with different defect site scenarios in the structures. Although the RSD worsened for all geometries, still the very best fit was obtained for nanoslabs with 1.3 nm along *a* and 4 nm along *b* and *c*.

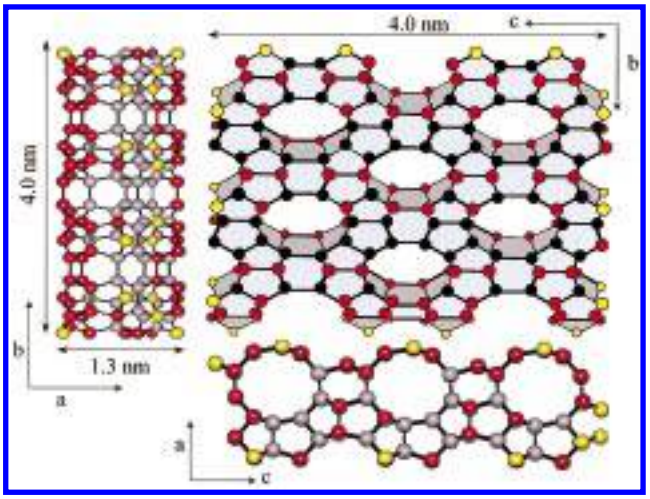

Figure 6. Crystallographically oriented elementary nanoslab of Silicalite-1. The Q^4, Q^3, and Q^2 type T-atoms are denoted as black, red, and yellow spheres, respectively.

Thermogravimetric analysis (TG) of the nanoslabs under oxidizing atmosphere reveals a high-temperature exothermic weight loss of 6.6 wt % between 513 and 673 K,[20] typical for TPA occluded in channel intersections.[29] Converted in template molecules per nanoslab, this comes down to 9 TPA molecules included into the slab. As every nanoslab contains nine channel intersections (Figure 6) the proposed model is supported by TG.

Nanoslabs and the Crystallization Mechanism of Silicalite-1 from "Clear" Solution. The combined results give evidence for a particle with very specific structure and dimensions (Figure 6). On this specific material, infrared spectra in the framework vibration region reveal a strong resemblance to MFI zeolites.[20] TEM studies result in the detection of the slablike geometry, and AFM comes up with one of the slab's dimensions being of the order of 1.2 ± 0.3 nm. Independently, the ^{29}Si MAS NMR spectrum can be best explained with a slab of MFI framework with dimensions of 1.3 nm along the crystallographic *a* direction of bulk MFI and 4 nm along the other directions, irrespective of the presence of defects. According to ^{13}C MAS NMR[20] and TG,[20] TPA is occluded and its concentration is in accordance with the proposed TPA−Silicalite-1 fragment. It will be shown later[24] that the XRS at 2.8° 2θ is also in excellent agreement with the presence of scattering bodies measuring 1.3 × 4 × 4 nm.

Aside from these arguments, stemming from the investigations on the extracted solid, further support for this structure comes from its relationship with precursor species, identified with liquid ^{29}Si NMR and in situ IR.[23] In situ XRS allows the direct observation of the transformation of precursors into nanoslabs by an association mechanism.[24]

The characterization of the nanoslabs proves that already at very early stages of the synthesis, the topology of MFI is realized. Furthermore, the system passes through a stage where identical particles of the same geometry and orientation are present. To gain further insight into the mechanism of MFI formation, several questions have to be addressed: (i) How is the hydrolysis and condensation directed to the exclusive formation of the MFI topology? (ii) Why are nanoslabs with the observed dimensions selectively formed in the clear suspensions before heating? (iii) How is Silicalite-1 formed upon heating of this nanoslab suspension? In the next article[23], the role of the TPA template molecule will be addressed. The formation of specific silicate precursor molecules will be presented. The transformation of precursors into nanoslabs is the subject of another article.[24]

Acknowledgment. This work is sponsored by the Belgian Government (IUAP−PAI program), the Flemish Fund for Scientific Research, and the Swedish Research Council for Engineering Sciences (TFR). P.J.G. acknowledges the Flemish Fund for Scientific Research for a research position, R.R. acknowledges K. U. Leuven for a postdoctoral fellowship.

References and Notes

(1) Flanigen, E. M.; Bennett, J. M.; Grose, R. W.; Cohen, J. P.; Patton, R. L.; Kirchner, R. M.; Smith, J. V. *Nature* **1978**, *271*, 512.
(2) Derouane, E. G.; Detremmerie, S.; Gabelica, Z.; Blom, N. *Appl. Catal.* **1981**, *1*, 201.
(3) Testa, F.; Szostak, R.; Chiappetta, R.; Aiello, R.; Fonseca, A.; Nagy, J. B. *Zeolites* **1997**, *18*, 106.
(4) Persson, A. E.; Schoeman, B. J.; Sterte, J.; Otterstedt, J.-E. *Zeolites* **1995**, *15*, 611.
(5) Persson, A. E.; Schoeman, B. J.; Sterte, J.; Otterstedt, J.-E. *Zeolites* **1994**, *14*, 557.
(6) Davis, M. E.; Lobo, R. F. *Chem. Mater.* **1992**, *4*, 756.
(7) Gies, H.; Marler, B. *Zeolites* **1992**, *12*, 42.
(8) Groenen, E. J. J.; Kortbeek, A. G. T. G.; Mackay, M.; Sudmeijer, O. *Zeolites* **1986**, *6*, 403.
(9) Jacobs, P. A.; Derouane, E. G.; Weitkamp, J. *J. Chem. Soc., Chem. Commun.* **1981**, 591.
(10) Chang, C. D.; Bell, A. T. *Catal. Lett.* **1991**, *8*, 305.
(11) Burkett, S. L.; Davis, M. E. *J. Phys. Chem.* **1994**, *98*, 4647.
(12) Schoeman, B. J.; Sterte, J.; Otterstedt, J.-E. *Zeolites* **1994**, *14*, 568.
(13) Schoeman, B. J. *Zeolites* **1997**, *18*, 97.
(14) Watson, J. N.; Iton, L. E.; Keir, R. I.; Thomas, J. C.; Dowling, T. L.; White, J. W. *J. Phys. Chem. B.* **1997**, *101*, 10094.
(15) Regev, O.; Cohen, Y.; Kehat, E.; Talmon, Y. *Zeolites* **1994**, *14*, 314.
(16) de Moor, P.-P. E. A.; Beelen, T. P. M.; van Santen, R. A. *Microporous Mater.* **1997**, *9*, 117.
(17) Dokter, W. H.; van Garderen, H. F.; Beelen, T. P. M.; van Santen, R. A.; Bras, W. *Angew. Chem.* **1995**, *34*, 73.
(18) Beelen, T. P. M.; Dokter, W. H.; van Garderen, H. F.; van Santen, R. A. In *Synthesis of Porous Materials, Zeolites, Clays, and Nanostructures*; Occelli, Kessler, Eds.; Dekker Inc.: New York, 1997; p 59.
(19) Schoeman, B. J. *Stud. Surf. Sci. Catal.* **1997**, *105*, 647.
(20) Ravishankar, R.; Kirschhock, C.; Schoeman, B. J.; Vos, D. D.; Grobet, P. J.; Jacobs, P. A.; Martens, J. A. *Proceedings of the 12th International Zeolite Conference*; Treacy, Marcus, Bisher, Higgins, Eds.; Materials Research Society: Pennsylvania, 1999; Vol. III, p 1825.
(21) Schoeman, B. J. *Microporous Mesoporous Mater.* **1998**, *22*, 9.
(22) Schoeman, B. J. *Zeolites* **1997**, *18*, 97.
(23) Kirschhock, C. E. A.; Ravishankar, R.; Verspeurt, F.; Grobet, P. J.; Jacobs, P. A.; Martens, J. A. *J. Phys. Chem B* **1999**, *103*, 4965.
(24) Kirschhock, C. E. A.; Ravishankar, R.; Van Looveren, L.; Jacobs, P. A.; Martens, J. A. *J. Phys. Chem B* **1999**, *103*, 4972.
(25) Shoeman, B. J.; Regev, O. *Zeolites* **1996**, *17*, 447.
(26) Ravishankar, R.; Kirschhock, C.; Schoeman, B. J.; Vanoppen, P.; Grobet, P. J.; Storck, S.; Maier, W. F.; Martens, J. A.; De Schryver, F. C.; Jacobs, P. A. *J. Phys. Chem. B.* **1998**, *102*, 2633.
(27) Cresge, C. T.; Leonowicz, M. E.; Roth, W. J.; Vartuli, J. C.; Beck, J. S. *Nature* **1992**, *359*, 710.
(28) Kokotailo, G. T.; Lawton, S. L.; Olson, D. H.; Meier, W. M. *Nature* **1978**, *272*, 437.
(29) Price, G. D.; Pluth, J. J.; Smith, J. V.; Araki, T.; Bennett, J. M. *Nature* **1981**, *292*, 818.